Combustion and Flame 222 (2020) 18–26

Contents lists available at ScienceDirect

Combustion and Flame

journal homepage: www.elsevier.com/locate/combustflame

Microgravity combustion of polyethylene droplet in drop tower

Peiyi Sun[a], Chuanjia Wu[b,c], Feng Zhu[b,c], Shuangfeng Wang[b,c,*], Xinyan Huang[a,**]

[a] Department of Building Services Engineering, The Hong Kong Polytechnic University, Hong Kong, China
[b] Key Laboratory of Microgravity, Institute of Mechanics, Chinese Academy of Sciences, Beijing 100190, China
[c] School of Engineering Science, University of Chinese Academy of Sciences, Beijing 1000490, China

ARTICLE INFO

Article history:
Received 1 March 2020
Revised 10 August 2020
Accepted 18 August 2020
Available online 31 August 2020

Keywords:
Droplet combustion
Burning-rate constant
Spacecraft fire safety
Thermoplastic droplet
Comet flame

ABSTRACT

Microgravity experiments of polyethylene (PE) droplet combustion were conducted by a 3.6-s drop tower with the gravity level of 10^{-3}~10^{-4} g to investigate the burning behaviors and fire hazards of molten thermoplastics in the spacecraft. Pre-ignited droplets with a diameter of about 3 mm were continually generated and detached from burning PE tubes. Once the drop capsule started free-fall, droplets entered the microgravity environment with an initial velocity of 10–35 cm/s (Stage I). A comet-shape flame with an intense bubbling and ejecting process of the moving droplet was observed, and the burning-rate constant (K) was found around 2.6 ± 0.3 mm^2/s. After the droplet landed on the floor, it could rebound with a near-zero velocity, showing as a spherical flame (Stage II). The combustion of PE droplet followed the classical d-square law with K = 1.3 ± 0.1 mm^2/s. The measured large burning-rate constant (or the volume shrinkage rate) of the moving droplet was caused by the robust bubbling process, which reduced the bulk density of molten PE and ejected unburnt fuel (about 25% of total mass loss). However, the actual mass burning rate of the PE droplet should be smaller than most hydrocarbon liquids because of a smaller mass-transfer number ($B \approx 2$). The flame burning rate of PE droplet is 4 ± 1 g/m^2-s per unit flame-sheet area that may be used to estimate the fuel mass-loss rate and fire heat release rate in microgravity. This novel microgravity combustion experiment on the thermoplastic droplet could expand the physical understanding of fire risk and hazard of plastic material in the spacecraft environment.

1. Introduction

The microgravity environment allows for an analytical description of the droplet combustion process by eliminating the buoyancy and natural convection [1]. The classical theory of one-dimensional (1-D) droplet combustion was first formulated by Spalding and Godsave in the early 1950s [2,3]. Since then, numerous microgravity experiments and numerical simulations have been performed subsequently to understand the combustion of liquid fuel droplets, as well as to verify and update the classical d-square law [2,3]. A wide range of droplet sizes up to 5 mm and fuel types, e.g., heptane, octane, diesel, methanol, have been tested, which have been reviewed in detail (e.g. [4–9]).

In addition to liquid-fuel droplets, the combustion of plastic spherical fuels in a solid phase was found roughly following the classical d-square law even if burning in normal gravity [10,11]. Some unique burning behaviors of plastic fuels, like bubbling and bursting, were found in burning three different plastic materials, polymethylmethacrylate (PMMA), polypropylene (PP), and polystyrene (PS), with diameters from 2 to 6.35 mm in low-gravity aircraft experiments [12,13]. Recently, a series of drop tower experiments on the PMMA sphere with a diameter of 10–40 mm were conducted to investigate the curvature effect on the flame extinction of solid fuels in microgravity [14]. Nevertheless, in all these experiments, spherical plastic fuels either were thermosets or did not fully melt into the liquid, so that the condensed-phase heat transfer will play an important role in the burning phenomenon [15].

Different from thermosetting polymers (e.g., cast PMMA), thermoplastic polymers, such as the polyethylene (PE), will first melt into liquid before ignition. Thus, the burning of molten thermoplastics is close to liquid fuel combustion, although the pyrolysis of melts is fundamentally different from the evaporation of liquid [16]. On Earth, the molten and burning thermoplastics tend to develop the flooring [17] and dripping [18,19] as driven by gravity. In microgravity, the burning thermoplastic materials tend to shrink into a ball under the surface tension force [20,21], which behaves like the classical droplet combustion. Today, thermoplastic

* Corresponding author at: Department of Building Services Engineering, The Hong Kong Polytechnic University, Hong Kong, China.
** Corresponding author.
E-mail addresses: sfwang@imech.ac.cn (S. Wang), xy.huang@polyu.edu.hk (X. Huang).

https://doi.org/10.1016/j.combustflame.2020.08.032
0010-2180/

Nomenclature

Symbols

A	area (m^2)
B	mass transfer number (-)
c_p	specific heat (kJ/kg-K)
d	diameter (mm)
D	mass diffusivity (mm^2/s)
Δh_c	heat of combustion (MJ/kg)
Δh_{py}	heat of pyrolysis (MJ/kg)
k	conductivity (W/m-K)
K	burning-rate constant (mm^2/s)
Le_{mix}	mixed Lewis number (-)
$\dot{m}$	mass-loss rate (kg/s)
$\dot{m}''$	mass flux (g/m^2-s)
Nu	Nusselt number (-)
PE	polyethylene
Pr	Prandtl number (-)
Re	Reynolds number (-)
t	time (s)
T	temperature (K)
v	velocity (cm/s)
V	volume (mm^3)
Y	mass fraction (-)

Greeks

η	pyrolysis efficiency (%)
ν	stoichiometric air-fuel ratio (-)
ρ	density (kg/m^3)

Subscripts

0	initial
I/II	stage one/two
∞	ambient
e	end or ejection
f	flame
F	fuel (gas)
g	gas
h	droplet height
i	inner region of flame
l	liquid fuel
l-g	liquid-gas interface
o	outer region of flame
O	oxidizer
py	pyrolysis
s	droplet surface
w	droplet width

materials are widely used for wire insulations and electrical devices aboard the spacecraft [22]. Thus, it is important to examine the combustion of thermoplastic droplets and its fire risk in microgravity spacecraft.

So far, very limited microgravity combustion experiments are available for the thermoplastic droplet. Most thermoplastics are in the solid phase at room temperature and have high melting and pyrolysis points. Thus, the time required for melting the entire PE particle into a liquid droplet and forming a stable flame takes several seconds, which is comparable to the short microgravity period of the drop tower. For example, the ignition delay time of PE thin-film almost took the entire microgravity time [23]. Although plastic fuels can be ignited and generate dripping before the microgravity time, the droplet will detach under gravity in a random fashion. Thus, it is challenging to heat, melt uniformly, and ignite the thermoplastic droplet, and synchronize the droplet detachment time with the free-fall time.

In this work, the microgravity combustion of molten PE droplet was studied in a 3.6-s drop tower with a gravity level of 10^{-3}–10^{-4} g. The pre-ignited PE droplets were continuously generated and detached from burning wires. The burning rates of PE droplets with and without forced flow were measured, which were verified against the classical d-square law and compared with liquid-fuel droplets. The unique phenomena of the PE droplet combustion, such as rebound, sliding, bubbling, and bursting (or ejecting), were discussed, which could shed light on fire hazards in spacecraft environments.

2. Experimental methods

The experiments were conducted in the 3.6-s drop tower in the National Microgravity Laboratory of China (NMLC), which offers a microgravity level of about 10^{-3}~10^{-4} g for the single-capsule test [24]. The effective space inside the sealed capsule was about 1 m^3, so that it includes about 300 g oxygen under the oxygen concentration of 21% and the pressure of 1 atm (Fig. 1(a)). Thus, for a short burning duration, the influence of oxygen depletion by combustion could be neglected. Inside the capsule, there was a test frame with the ceiling and floor made of the aluminum panel and all sides open to the capsule (Fig. 1(b)). Within the test frame, a customized PE droplet generator, high-speed camera, and data collection system were installed (Fig. 1(b-d)). Once all preparation works were finished, the scaled capsule was held by an electromagnetic head that could be elevated to the top of the tower for controlling the release.

In previous normal-gravity dripping experiments [18,19], the fully liquidized PE droplet attached to a flame was generated from the burning PE tubes. The ignition time of the PE tube by an electric coil or a torch took about 10 s. After ignition, it took a few more seconds for the flame to develop, melt PE completely, and then flow along the tube or form a detached PE droplet. As the microgravity period in the drop tower test was limited to 3.6 s, igniting PE like previous 1 g tests before the free fall was also preferred. Nevertheless, unlike the typical liquid fuel droplet, with gravity, it was also extremely difficult to hold the PE particle/droplet (such as by fine wires) during heating, melting, and burning processes. It is because the surface tension of PE dramatically changed with the temperature and the bubbling phenomenon and became non-uniform inside. Meanwhile, it was almost impossible to control the release time of the drop capsule simultaneously when PE was fully molten while just before detached, as proved by six failed preliminary drop tests.

To better control the time of dripping and the release of the capsule, a new statistic approach was adopted. Four PE tubes with an inner diameter of 3 mm and an outer diameter of 4 mm were placed vertically and held by a corundum core. They were ignited simultaneously by the nichrome coil, as shown in Fig. 1(c-d). Then, the burning liquid PE flowed down along the core, detached as a molten-PE droplet with a flame. The PE droplet had an initial diameter (d_0) of 3.0 ± 0.5 mm and a dripping frequency of 3 Hz. With four burning wires, the overall dripping frequency was 12 Hz, so about 4 PE droplets could appear in the air at the same time. Then, even if the capsule was released randomly, there was a high probability of having 1~2 burning PE droplets in the air while entering the microgravity environment.

Another ten drop tests were conducted with this new method of generating PE droplets, in which five tests successfully captured six droplet combustion processes in microgravity, and four droplets burned for more than 1 s. Particularly, two PE droplets bounced back after landed on the floor, showing two stages of burning. Their moving and burning processes were recorded by a high-speed camera (AOS TRI-VIT) at 500 fps with a resolution of about 0.1 mm/pix. An LED backlight from the side was applied to help

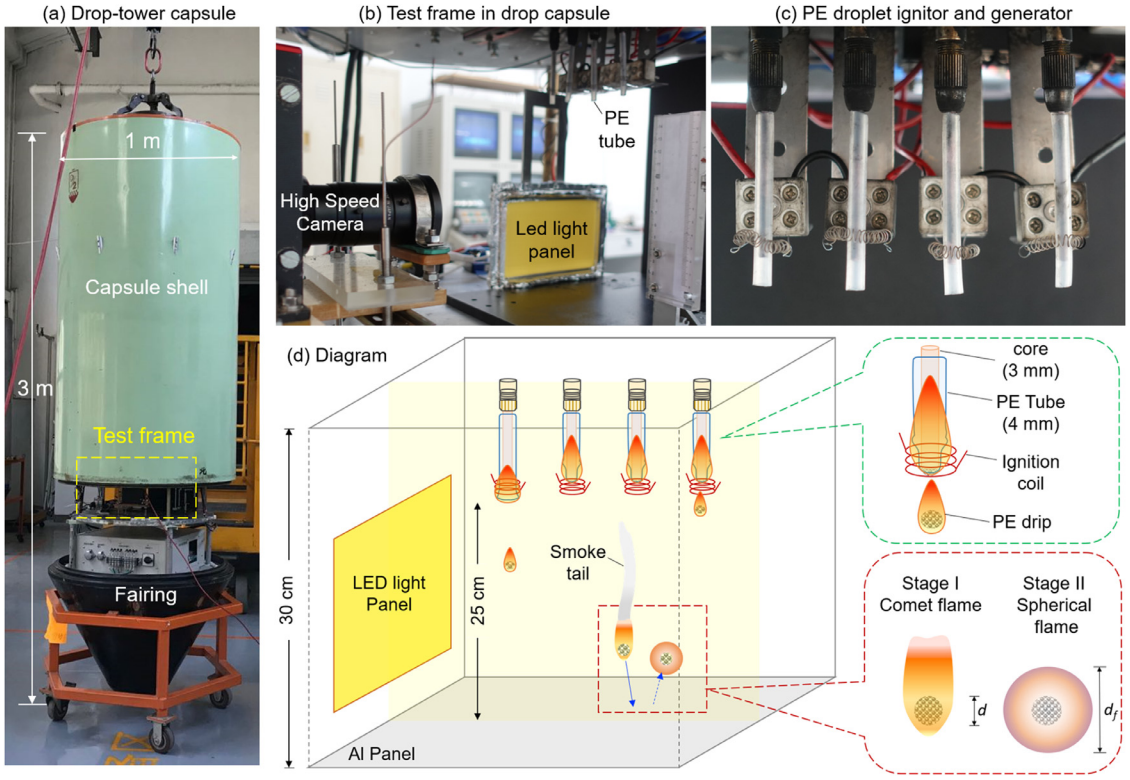

Fig. 1. (a) The single drop capsule before sealing, (b) Test frame within the drop capsule, (c) PE tube ignitor and droplet generator, and (d) the diagram of the experiment setup and PE droplet combustion process.

visualize the droplet within the flame. All recorded videos were analyzed frame by frame with an in-house MATLAB code to measure the velocity of PE droplet and smoke, as well as the diameter of droplet and flame.

3. Results and discussions

3.1. Flame shapes

3.1.1. Comet flame of moving droplet

Figure 2(a) shows the trajectory and the burning process of the PE droplet in the microgravity drop period. Because an initial downward velocity was required for the droplet to detach from the parent fuel, the PE droplet had an initial velocity. Thus, the Stage-I burning of the moving droplet showed a comet-shaped flame. The observed yellow flame might be the soot shell or the inner layer of the flame sheet, where the outer blue flame layer was not visualized by the current high-speed imaging sensor. The soot radiation could also contribute to the pyrolysis of the PE droplet. There was inevitably a small flow induced by flames on PE tubes, so the burning environment was semi-quiescent. Nevertheless, such a background airflow was no more than 5 cm/s, based on the measurement of the smoke motion.

Moreover, a strong bubbling process was found inside the PE droplet, so the PE droplet was highly porous and different from conventional droplet combustion [5]. This intense bubbling process led to strong bursts (or ejections [25]) of tiny PE droplets (Fig. 2(b)). Most of the bursts were too weak to penetrate the flame sheet but only deformed the local flame shape and burnt out within the flame. Nevertheless, some ejected fuel (mostly tiny liquid PE particles) was strong enough to penetrate through the flame sheet and even change the trajectory of the moving droplet. The frequency of these strong bursts was measured to be 11 ± 2 Hz. Previously, bubbling and bursting were also found in the normal-gravity combustion of PE droplet [11], and the microgravity combustion of PMMA [26], PP, and PS, where PP had a bursting frequency of 5 Hz [12].

Figure 2(c) shows a typical evolution of droplet velocity (v) within the comet flame. Before detaching from the PE tube ($t_I < 0$), the molten PE flowed downward and formed a dripping flow, as it was dragged by the gravity, which helped overcome the surface-tension and viscous forces. The moment of detachment coincided with the moment of capsule drop ($t_I = 0$) when the PE droplet reached its maximum velocity of about 35 cm/s. Afterward, the PE droplet started to move in the semi-quiescent air and continuously decelerate because of the air drag. Such a deceleration was calculated as about 0.2 m/s^2 (or 0.02 g). Right after the detachment, the flame may not be able to cover the entire droplet. However, during the deceleration process, the droplet became fully covered by the comet flame.

Behind the moving droplet, there was a smoke tail leaking from the tip-open comet flame (Fig. 2(a)), and the flame length became relatively shorter (Fig. 2(d)). The smoke could primarily be the condensed tiny PE particles. The main components of PE pyrolysis gas include ethane (27.4%), propane (26.6%), and methane (22.7%), while ethylene is 1.4%, and large molecules (>C_7) is 1.9% [27]. Thus, the smoke tail may also include some unburnt pyrolysis gases of large molecular weights like aromatic compounds [28], as well as soot. The soot concentration might also increase with decreasing co-flow velocity. The existence of smoke tail indicated the comet flame reached its smoke point. Similar tip-open flame phenomena had been observed in many past microgravity tests, which may be associated with the extinction of the flame near its tip due to intense radiative heat losses from soot [29–31]. More likely, the tip-open flame can be considered as a blow-off phenomenon, which can be quantified by a critical Damkohler number, where the radiatively cooled flame increases the chemical time to be comparable with the flow residence time [6]. The smoke-point flame length

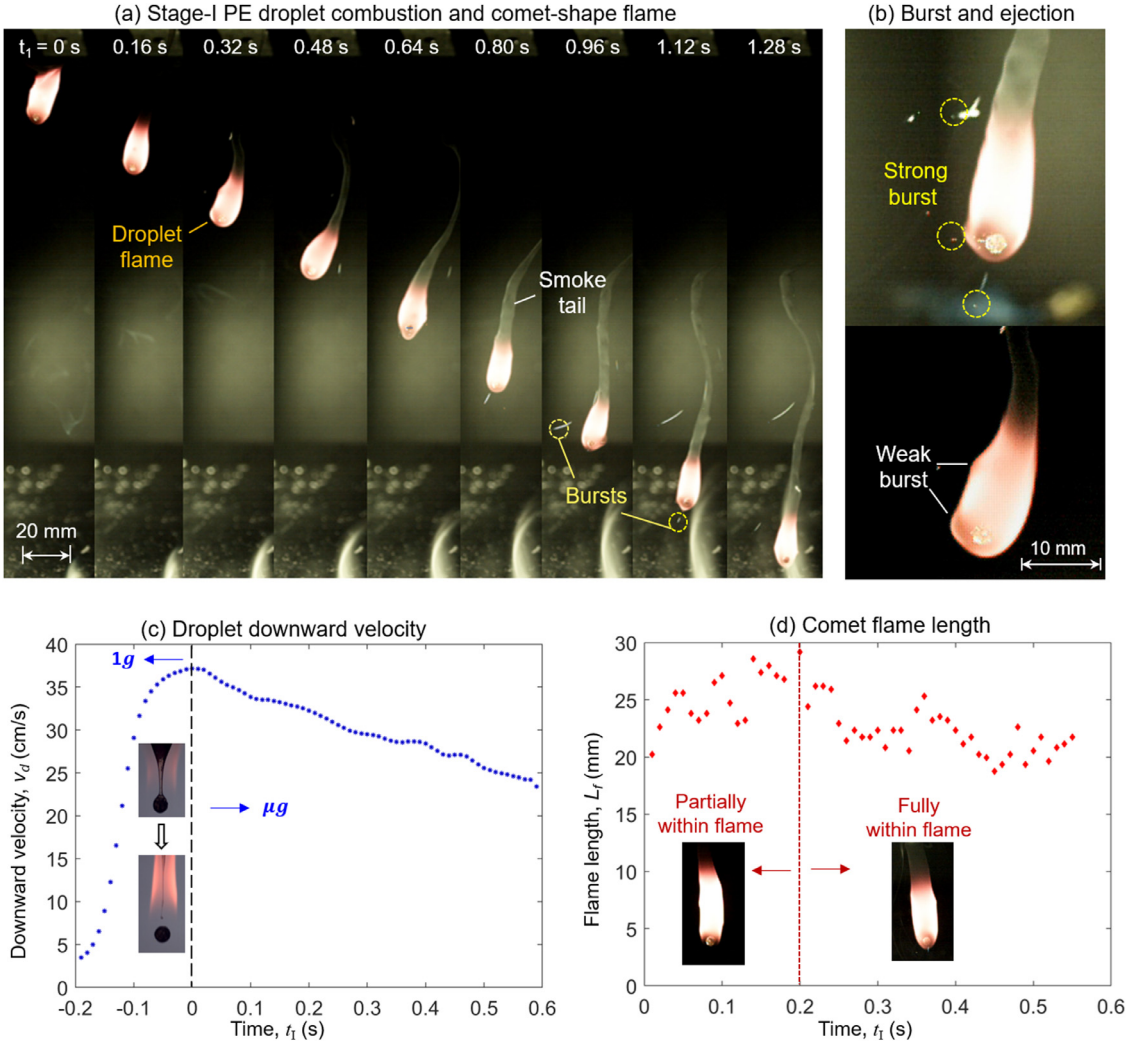

Fig. 2. (a) Snapshots of Stage-I microgravity combustion of the PE droplet and comet-shaped flame (Video S1), (b) bubbling, burst, and ejection processes, (c) velocity of PE droplet, and (d) length of comet flame. (For interpretation of the references to color in this figure, the reader is referred to the web version of this article.)

in microgravity was correlated positively with the co-flow velocity [31–33]. Comparison between Fig. 2(c) and (d) shows a similar trend between the droplet velocity (or relative flow velocity) and the flame length.

3.1.2. Spherical flame of semi-quiescent droplet

Once landed on the floor, the PE droplet can rebound as an intact liquid ball occasionally (Fig. 3(a) and Video S1), and such a rebound process was observed twice out of six droplets. Once rebounded ($t_{II} = 0$), almost a perfect spherical flame can be observed in the Stage-II droplet combustion. After the rebound, the upward velocity of the droplet became minimal ($v < 8$ cm/s) and comparable to the background airflow velocity (~5 cm/s), as shown in Fig. 3(b). Due to the air drag, the velocity of rebounded droplet decreased to near zero at $t_{II} = 0.65$ s with a similar deceleration of 0.1 m/s^2. Afterward, the droplet moved randomly, caused by the combined effect of bubbling bursts, air drag, and remaining microgravity.

Excluding the transition from the comet flame to spherical flame, the valid time of Stage-II burning is about 1 s. Compared to the Stage-I burning of the moving droplet, the droplet combustion in this semi-quiescent environment is more stable, because of a larger flame standoff distance and a lower flame heat flux. For the same reason, only a weak burst was observed, where ejected fuel vapor or tiny particles could not penetrate through the flame sheet, but only slightly change the motion of the near-stationary droplet.

On the other hand, some other landed PE droplets had a larger initial downward velocity. Thus, after landing, they were compressed and eventually absorbed by the molten layer on the floor (Fig. 4(a) and Video S2), which was similar to the phenomenon frequently observed in normal gravity [34]. On the floor, previous PE droplets re-solidified into a random shape, which guided later droplets to move randomly after landing. Figure 4(b) and Video S3 show a droplet sliding horizontally on the floor after landing. It is because PE droplet was always enveloped by the pyrolysis gas layer that prevented direct contact with the cooler floor. In other words, this is an inverse Leidenfrost phenomenon[1] [35]. The pyrolysis gas layer was also expected to play an essential role in the rebound process (Fig. 3(a)). Although the microgravity environment limits the overall motion of fuel, such an inverse Leidenfrost phenomenon could increase the mobility of burning fuel droplets and create an additional fire risk for spacecraft.

[1] Leidenfrost phenomenon indicates a cold droplet floats above the hot object, while here is a hot droplet floating above the cold object.

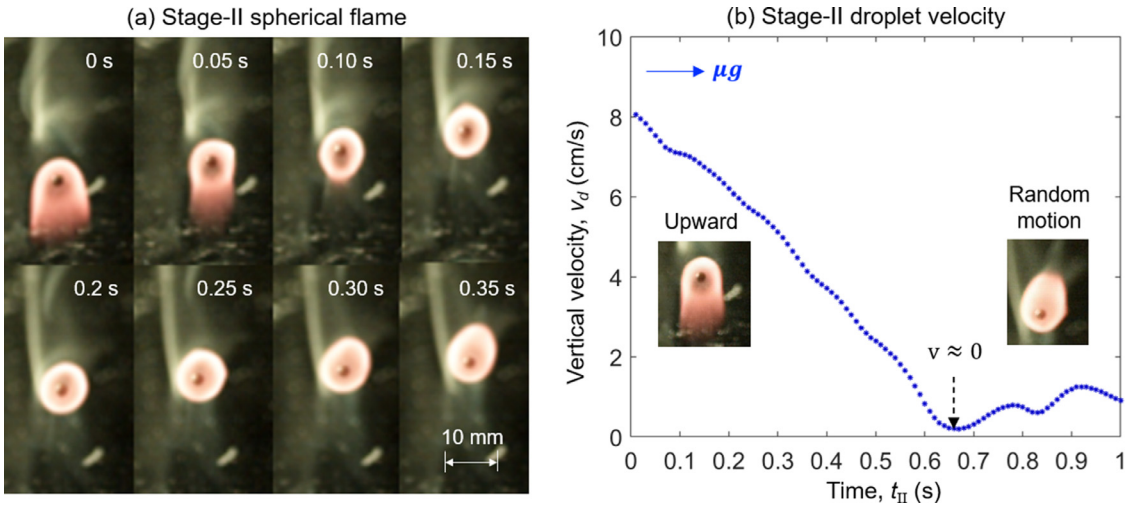

Fig. 3. High-speed snapshots of the rebounding burning PE droplets after reaching the ground, (a) the Stage-II spherical flame after rebound (Video S1), and (b) velocity of PE droplet after the rebound.

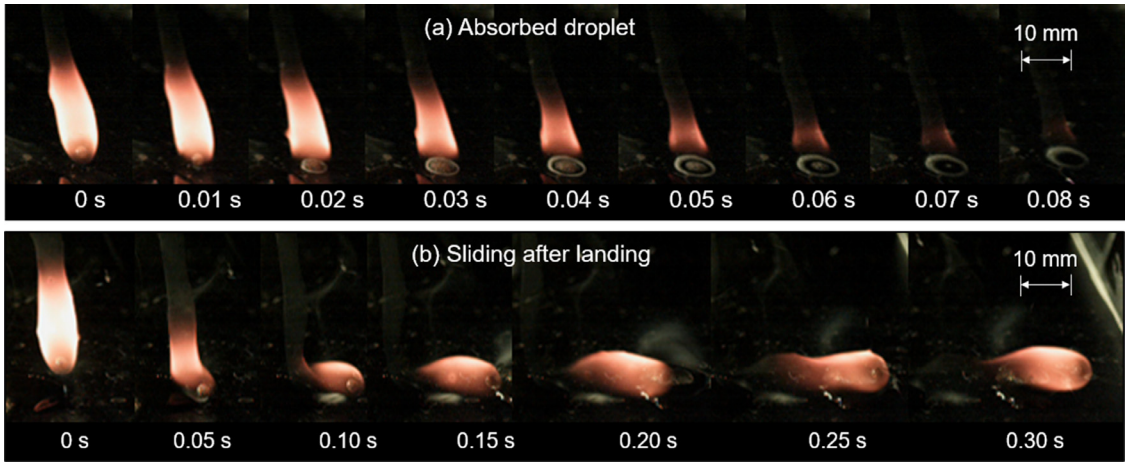

Fig. 4. High-speed snapshots of other possible phenomena after the burning PE droplets reaching the ground, (a) absorbed droplet (Video S2), and (b) the sliding droplet (Video S3) under the inverse Leidenfrost effect.

3.2. Burning rates

During the microgravity combustion, the PE droplet was not in a perfectly spherical shape but varied continuously with time, mainly because of the strong internal bubbling and bursting processes. Especially right after the detachment and rebound, the flame may not fully cover the droplet (Fig. 2(a,d)), where the variation of droplet shape and diameter was irregular, so the droplet diameter in these transitions was not considered in the calculation of the burning rate. Through the imaging process by MATLAB, the time evolution of width and height, as well as the eccentricity of the PE droplet, was examined. Despite the imperfect sphere, the mean eccentricity of PE droplet was less than 0.2, indicating that shape was close to a sphere (zero eccentricity). As a first approximation, the diameter of equivalent spherical diameter (d) was calculated based on the volume conservation as

$$V = \frac{1}{6}\pi d_h d_w^2 = \frac{1}{6}\pi d^3 \quad (1)$$

Figure 5 plots the measured the d-square of all PE droplets (Stages I and II). For all experiments, the d-square of PE droplet decreased linearly with the time, agreeing with the classical d-square law. The measured data have a relatively larger variation than those of other liquid fuel droplets [4,5,7,9], which is attributed to the shape change induced by bubbling and bursting. Note that even for the droplet combustion in normal gravity, the d-square law was roughly satisfied, e.g. [11,36], although the buoyancy flow could change with the size and shape of droplet flame.

Table 1
Measured droplet initial diameter (d_0), end diameter (d_e), and burning-rate constant (K).

Test	Stage	d_0 (mm)	d_e (mm)	K (mm^2/s)
1	I	3.20	3.06	2.6 ± 0.3
2	I	3.32	3.15	2.6 ± 0.2
3	I	3.35	2.92	2.6 ± 0.1
4	I	3.38	3.23	2.6 ± 0.3
5	II	2.10	1.80	1.3 ± 0.1
6	II	2.03	1.74	1.3 ± 0.1

Table 1 summarizes the initial diameter (d_0), end diameter (d_e), and burning-rate constant (K) measured in each trial. For the moving PE droplet in Stage I, the burning-rate constant was K_I =2.6 ± 0.3 mm^2/s, and for the semi-quiescent PE droplet in Stage II, K_{II} =1.3 ± 0.1 mm^2/s, where the uncertainty of repeating experiments was reasonable. Because the flame heat flux was enhanced by the droplet motion, the burning-rate constant in Stage I was larger, as expected. For the droplet combustion of most hydrocarbon liquids in the literature, K < 1 was often found [5,7,9,37], so

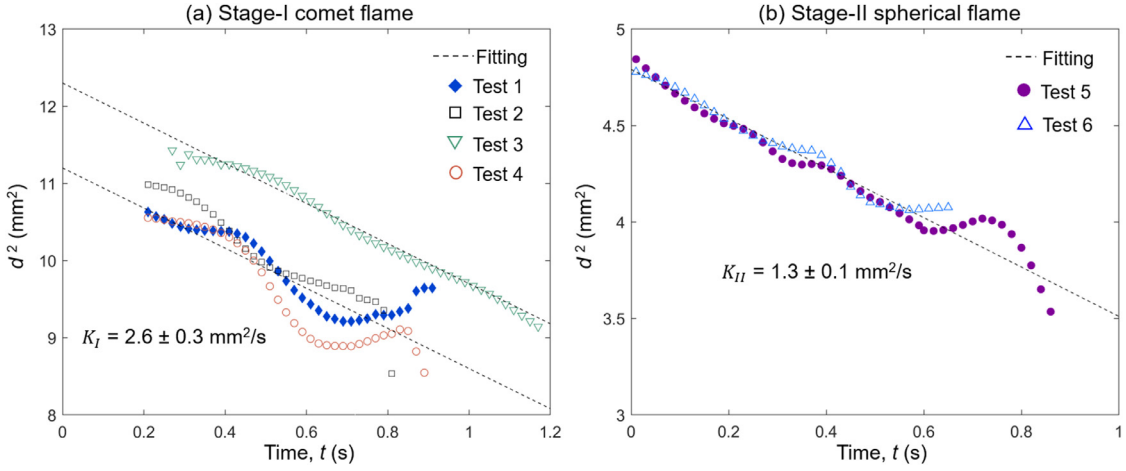

Fig. 5. Measured d-square for the microgravity combustion of PE droplets, (a) the Stage-I comet flame, and (b) the Stage-II spherical flame after the rebound, where different symbols represent different tests listed in Table 1, and the least-square fit is used to estimate the average burning rate constant.

that PE droplet has a much larger burning-rate constant. For example, even under a forced flow of 5 cm/s, the burning-rate constant of a methanol droplet was only 0.74 mm^2/s [9].

In normal gravity, the burning-rate constant of PE spheres with 1 or 2 mm diameter was previously found to be 2.5 mm^2/s [10]; and for PMMA sphere, the burning-rate was 2.2 mm^2/s at 1 atm [11], which were close to K_I =2.6 ± 0.3 mm^2/s in Stage I. It is because under the normal gravity, the droplet flame could induce a buoyancy flow of about 30~50 cm/s that was comparable to the droplet velocity in Stage I (Fig. 2(c)). Yang [12,13] studied the combustion of 3 mm PMMA spheres in parabolic flight (10^{-2} g) with three oxygen concentrations. The measured the burning-rate constant at an oxygen level of 19.9% was 1.3 mm^2/s, which was close to K_{II} =1.3 ± 0.1 mm^2/s of semi-quiescent PE droplet in Stage II at the oxygen level of 21%.

The burning-rate constant depends on the processes of phase change and mass transfer. The classical expression of the mass-transfer number (B) [1,4,5,7] can be applied for the PE droplet as

$$B_{PE} = \frac{\Delta h_c/\nu + c_{pg}(T_\infty - T_{py})}{\Delta h_{py}} \approx 2 \tag{2}$$

As methane and ethane are the main compositions of PE pyrolyzates [38], their properties are adopted for gaseous fuel, where $\Delta h_c \approx$ 50 MJ/kg is the heat of combustion; $\nu = 14.8$ is the stoichiometric air-fuel ratio; $T_{py} \approx$ 673 K is the pyrolysis temperature of PE [16], and the pyrolysis heat of PE is $\Delta h_{py} \approx$ 1 MJ/kg [39]. By estimating the flame temperature as $T_f \approx$ 2000 K, the average temperature between the flame and the droplet surface is $(\bar{T}) = 0.5(T_p + T_f) \approx$1300 K. The specific heat of fuel $c_{pg} = c_{pF}(\bar{T}) \approx$ 3 kJ/kg-K is used for the mixture of methane, ethane, other heavy hydrocarbons, and tiny condensed PE particles, where the evaporation is controlled by the heat transfer in the flame inner region [6,40,41].

The value of B here is comparable to the literature value and other polymers [11,16], which is much smaller than most liquid fuels, such as methanol ($B \approx$ 3.0), heptane ($B \approx$ 8.6), and diesel ($B \approx$ 11) [5,6]. It is because the pyrolysis heat (Δh_{py}) and temperature (T_{py}) of PE in Eq. (2) are much larger than the heat of evaporation and boiling point of most liquid fuels. For the liquid polymer fuel, the surface temperature continues to increase even above the pyrolysis point with a strong the internal heat convection, which is neglected in Eq. (2). The fuel mass loss rate ($\dot{m}_F$) and mass flux ($\dot{m}_F''$) increases with B as

$$\dot{m}_F = -\rho_l \frac{\mathrm{d}V}{\mathrm{d}t} = \frac{\pi}{4}\rho_l K d = \frac{2\pi k_{l-g} d}{c_{pg}} \ln(1+B) \tag{3a}$$

$$\dot{m}_F'' = \frac{\rho_l K}{4d} = \frac{2k_{l-g}}{dc_{pg}} \ln(1+B) \tag{3b}$$

where ρ_l is the liquid fuel density, and $k_{l\text{-}g}$ is the local thermal conductivity for the liquid-gas interface. Therefore, given a droplet diameter, the mass burning rate of the PE droplet should be lower than those of heptane and methanol droplets because of the smaller B number.

Nevertheless, it is unexpected the measured burning-rate constant of semi-quiescent PE droplet in Stage II, K_{II} =1.3 ± 0.1 mm^2/s, to be larger than most hydrocarbon liquid fuels with a larger B. Different from the mass-based burning rate, the burning-rate constant (K) in d-square law is derived from the volume change of droplet. In other words, it is essentially a shrinkage rate of the spherical volume as

$$K = -\frac{\mathrm{d}(d^2)}{\mathrm{d}t} = -\frac{4}{\pi d}\left(\frac{\mathrm{d}V}{\mathrm{d}t}\right) = \frac{4}{\pi d \rho_l}\dot{m}_F \tag{4a}$$

Therefore, the only possible reason for a smaller mass burning rate of PE droplet having a large burning-rate constant should be the decrease in liquid PE density (ρ_l). As a strong bubbling process is observed inside the PE droplet, it is expected that the droplet is porous and has a lower density.

For the Stage-II droplet combustion with the semi-quiescent droplet, the burning-rate constant follows the classical expression [5]

$$K_{II} = \frac{8k_{l-g}}{\rho_l c_{pg}} \ln(1 + B_{PE}) = 1.3\mathrm{mm}^2/\mathrm{s} \tag{4b}$$

where $B_{PE} = 2$ from Eq. (2). Because the existence of multi-phase fuel (complex pyrolysis gases and tiny condensed PE particles seen in Fig. 6) also promotes the heat transfer at the droplet surface, a relatively large effective thermal conductivity ($k_{l\text{-}g} \approx$ 0.23 W/m-K) [41,42] is chosen, considering that the thermal conductivity of methane is 0.17 W/m-K at 1000 K and 0.32 at 1300 K [42]. Then, the density of the porous bubbling PE droplet is calculated as about 560 kg/m^3, which is smaller than 930 kg/m^3 for the non-porous molten PE [39], but close to the previous measurement of PE drippings in normal gravity [18].

On the other hand, the Stage-I burning process of a moving droplet is equivalent to the droplet combustion under a forced

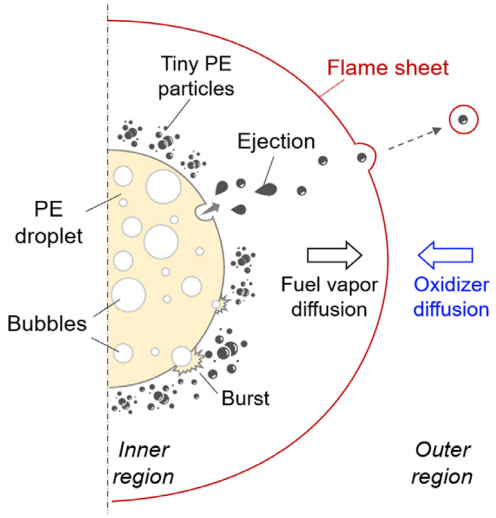

Fig. 6. Schematic diagram of PE droplet, flame, bubbling, burst, and ejection processes.

convective environment, and the burning-rate constant may be expressed as

$$K_I = \frac{4k_{l-g}Nu_I}{\rho_l c_{pg}} \ln(1+B_{PE}) = 2.6 \text{ mm}^2/\text{s} \tag{4c}$$

The influence of convective flow is considered by the Nusselt number (Nu) [43] as

$$Nu_I = 2 + 0.6Re^{1/2}Pr^{1/3} \approx 3.0 \pm 0.1 \tag{5}$$

where the mean velocity of PE droplet in Stage I is 25 ± 6 cm/s. By using the actual density of 560 kg/m^3 found in Stage II, the calculated burning-rate constant for Stage I is 2.0 ± 0.1 mm^2/s, which is still appreciable smaller than the experimental measurement of 2.6 ± 0.3 mm^2/s in Fig. 5(a). Therefore, there must be some other factor contributing to such a large burning-rate constant in Stage I.

As observed in Fig. 2(a,b) and Videos S1–3 and illustrated in Fig. 6, the violent bubbling phenomenon in Stage I results in the strong burst and frequent fuel ejections, which penetrate out of the flame sheet. Comparatively, bursts, and injections in Stage II (spherical flame) are weaker, which are not strong enough to penetrate the flame sheet. Therefore, it is possible to define a gasification or pyrolysis efficiency (η) to correct the burning rate by removing the mass loss induced by the strong ejection as

$$\eta = \frac{\text{combusted fuel}}{\text{gasified fuel}} = \frac{\dot{m}_{F,f}}{\dot{m}_F} = \frac{\dot{m}_{F,f}}{\dot{m}_{F,f}+\dot{m}_{F,e}} \tag{6a}$$

where the total fuel mass loss rate ($\dot{m}_F$) includes both the mass-loss rate due to strong ejections ($\dot{m}_{F,e}$) and the actual fuel burning rate in flame ($\dot{m}_{F,f}$). As the conventional equation only considers the mass loss caused by burning, the measured burning rate should divide the gasification efficiency to express the total mass loss. Moreover, according to Eq. (4a), the burning-rate constant is positively correlated with the mass burning rate. Therefore, the gasification efficiency should be added to modify the measure burning-rate constant as

$$\dot{m}_F = \frac{\dot{m}_{F,f}}{\eta} \propto \frac{K}{\eta} \tag{6b}$$

Note that all weak fuel burst and ejection in Stage II were consumed within the flame, so that $\eta_{II} \approx 1$. Then, the burning-rate constant of the PE droplet in Stage I in Eq. (4c) can be corrected as

$$K_I = \frac{4k_{l-g}Nu_I}{\rho_l c_{pg}\eta_I} \ln(1+B_{PE}) \tag{4d}$$

Accordingly, the gasification efficiency of Stage I can be estimated as

$$\eta_I = \frac{Nu_I}{2}\left(\frac{K_{II}}{K_I}\right) = 75 \pm 10\% \tag{6c}$$

In other words, about 75% of PE droplet is consumed by the flame, and the rest 25% of PE droplet is lost by the high-frequent strong ejections.

3.3. Flame standoff distance and burning flux

The diameter of the PE droplet and spherical flame in Stage II of two tests was measured by processing the high-speed images in MATLAB. Simultaneously, the flame standoff ratio (FSR), defined as the flame diameter (d_f) divided by the droplet diameter (d), can be theoretically estimated as:

$$\frac{d_f}{d} = \frac{\ln(1+B)}{\ln[(1+\nu)/\nu]} \tag{7a}$$

where the 'theoretical' value is found to be around 17, which is smaller than the 'theoretical' value (about 40) of a typical liquid hydrocarbon fuel flame [5]. Nevertheless, Fig. 7(a) shows that the experimentally measured FSR for PE droplet is about 4~5. It is much smaller compared to the measured FSR for typical liquid hydrocarbon fuels (about 10) [5] and methanol droplet (5~6) [44]. On the other hand, a smaller FSR of 3~4 was observed in the combustion of spherical PMMA [11].

The value of FSR is controlled by the mass transfer and strongly influenced by the diffusion coefficients of fuels and oxygen [10]. Usually, the quasi-steady droplet combustion theories over-predict the FRS by several folds [5]. There are two possible reasons for the relatively small FSR. Firstly, some pyrolysis gases of large molecular weight and even the tiny condensed PE particles in the flame inner region are more difficult to diffuse to the flame, as illustrated in Fig. 6. This is also called as the fuel vapor/particle accumulation effect and could be represented by the mixed Lewis number (Le_{mix}) [5,6,45] as

$$\frac{d_f}{d} = 1 + Le_{\text{mix}}\frac{\ln\left[1+c_{pF}\left(T_f-T_s\right)/\Delta h_{py}\right]}{\ln(1+Y_{O,\infty}/\nu_O)} \tag{7b}$$

$$Le_{\text{mix}} = \frac{(k/c_p)_i}{(\rho D)_o} \approx \frac{k_F/c_{pF}}{\rho_O D_O} \tag{8}$$

where subscripts i and o represent the flame inner and outer diffusive-convective regions, respectively. The mixed Lewis number is usually smaller than 1, due to the smaller thermal diffusion of fuel molecules inside the flame. Moreover, the value of Le_{mix} for the PE droplet flame could be even smaller, because the existence of tiny condensed PE particles not only increases the effective specific heat (c_{pF}) due to the additional phase change process, but also slows down the overall diffusion process (k_F) between the flame and the droplet. Note that k_F is an overall value that is different from $k_{l\text{-}g}$ at the liquid-gas interface in Eq. (3).

Secondly, because of the limitation of the current high-speed imaging sensor, the observed yellow spherical flame may not represent the outer boundary of the blue flame [12,46]. Thus, the measured flame diameter was likely under-estimated. Better measurements of droplet flame color and radiation will be conducted in future microgravity experiments with additional cameras.

Based on the measurement of flame shape and size, the flame-sheet area (A_f) of both the Stage-I comet flame and the Stage-II spherical flame can be estimated. Then, the flame burning flux

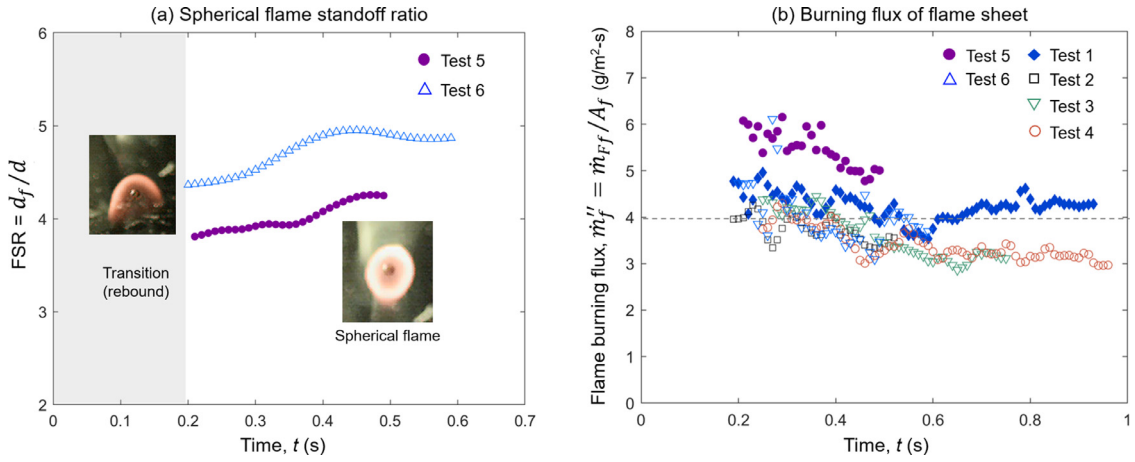

Fig. 7. (a) Flame standoff ratio for droplet combustion in stage II for Tests 5 and 6 in Table 1 and (b) the measured flame burning flux for both comet and spherical flame, where the ejected fuel is excluded in Stage I.

($\dot{m}_f''$), i.e., the burning rate per unit flame sheet area, can also be estimated as

$$\dot{m}_f'' = \frac{\text{Fuel burning rate}}{\text{Flame sheet area}} = \frac{\dot{m}_{Ff}}{A_f} = \begin{cases} \frac{\eta \dot{m}_F}{A_f} \text{ (I : comet flame)} \\ \frac{\dot{m}_F''}{FSR^2} \text{ (II : spherical flame)} \end{cases} \quad (9)$$

Fig. 7(b) shows the measured the flame burning flux of PE droplet for both stages, where the ejected tiny PE particles that penetrate the flame sheet is not considered in Stage I. Clearly, we found the average flame burning flux of PE droplet is $\dot{m}_f'' = 4 \pm 1$ g/m^2-s for both burning stages and all tests, which is close to the values of heptane (2–5 g/m^2-s [47,48]) and methanol (from 2.5 [49] to 5–9 g/m^2-s [50]). Considering the difficulty of measuring the fuel mass loss rate in microgravity (i.e., the regular scale fails), by knowing the flame burning flux of the specific fuel and measuring the flame-sheet area, it provides a method to estimate the fuel burning rate and the fire heat release rate in the microgravity spacecraft environment.

4. Conclusions

In this study, the combustion of the molten thermoplastic droplet has been tested under the microgravity drop tower. A unique experimental setup was designed to successfully produce the pre-ignited PE droplets with a diameter of 2~3 mm and a small initial velocity within less than 40 cm/s. Once the drop started, two stages of droplet combustion were observed,

(I) a comet-shape flame for a low-velocity droplet with strong bubbling and ejecting processes and the burning-rate constant (K) of 2.6 ± 0.3 mm^2/s; and
(II) a spherical flame after the rebound of the droplet with K of 1.3 ± 0.1 mm^2/s.

The combustion of all PE droplets followed the classical d-square law. The measured large burning-rate constant (or the volume shrinkage rate) for moving droplets is caused by the strong bubbling process, which reduces the bulk density of molten PE. A gasification efficiency was introduced, which estimated the ejected fuel that penetrated trough the comet flame to be about 1/4 of total mass loss. However, considering the higher pyrolysis point, larger heat of pyrolysis, and smaller mass-transfer number ($B \approx 2$), the actual mass burning rate of PE droplets should be smaller than the most hydrocarbon liquids. We found the flame burning flux of PE droplet to be 4 ± 1 g/m^2-s per unit flame sheet area that may be used to estimate the fuel mass-loss rate and fire heat release rate in microgravity. This novel microgravity combustion experiment could help understand the fire risk and hazard of plastic material in the spacecraft environment.

Declaration of Competing Interest

The authors declare that they have no known competing financial interests or personal relationships that could have appeared to influence the work reported in this paper.

Acknowledgments

This work is supported by National Natural Science Foundation of China under the Grant No. U1738117 and 51876183, the CAS Strategic Priority Research Program on Space Science (Nos. XDA04020410 and XDA04020202-10).

Supplementary materials

Supplementary material associated with this article can be found, in the online version, at doi:10.1016/j.combustflame.2020.08.032.

References

[1] H.D. Ross, Microgravity Combustion : Fire in Free Fall, Academic Press, 2001.
[2] G.A.E. Godsave, Studies of the combustion of drops in a fuel spray-the burning of single drops of fuel, Symp. (Int.) Combust. 4 (1953) 818–830, doi:10.1016/S0082-0784(53)80107-4.
[3] D.B. Spalding, The combustion of liquid fuels, Symp. (Int.) Combust. 4 (1953) 847–864, doi:10.1016/S0082-0784(53)80110-4.
[4] A. Williams, Combustion of droplets of liquid fuels: a review, Combust. Flame 21 (1973) 1–31, doi:10.1016/0010-2180(73)90002-3.
[5] C.K. Law, Recent advances in droplet vaporization and combustion, Prog. Energy Combust. Sci. 8 (1982) 171–201, doi:10.1016/0360-1285(82)90011-9.
[6] C.K. Law, Combustion Physics, Cambridge University Press, 2010.
[7] D.L. Dietrich, V. Nayagam, M.C. Hicks, P.V. Ferkul, F.L. Dryer, T. Farouk, et al., Droplet combustion experiments aboard the international space station, Microgravity Sci. Technol. 26 (2014) 65–76, doi:10.1007/s12217-014-9372-2.
[8] M. Ackerman, F. Williams, Simplified model for droplet combustion in a slow convective flow, Combust. Flame 143 (2005) 599–612, doi:10.1016/j.combustflame.2005.08.025.
[9] D.L. Dietrich, J.B. Haggard, F.L. Dryer, V. Nayagam, B.D. Shaw, F.A. Williams, Droplet combustion experiments in spacelab, Symp. (Int.) Combust. 26 (1996) 1201–1207, doi:10.1016/S0082-0784(96)80336-5.
[10] R.H. Essenhigh, W.L. Dreier, Combustion behavior of thermoplastic polymer spheres burning in quiescent atmospheres of air, Proceedings of the AlAA 51h AerosDace Sciences Meeting (1967), doi:10.2514/6.1967-103.

[11] T. Migita, T. Yamahata, P. Strempfl, T. Matsuoka, Y. Nakamura, Methodology to achieve pseudo 1-D combustion system of polymeric materials using low-pressured technique, Fire Technol. (2020), doi:10.1007/s10694-019-00877-x.
[12] J.C. Yang, A. Hamins, M.K. Donnelly, Reduced gravity combustion of thermoplastic spheres, Combust. Flame 120 (2000) 61–74, doi:10.1016/S0010-2180(99)00084-X.
[13] Yang J.C., Hamins A., Donnelly M.K. Combustion of a Polymer (PMMA) Sphere in Microgravity. NASA/CR–1999-209403 and NISTIR 6331 1999.
[14] C. Wu, P. Sun, X. Wang, X. Huang, S. Wang, Flame extinction of spherical PMMA in microgravity: effect of fuel diameter and conduction, Microgravity Sci. Technol. (2020) [under Review].
[15] M. Endo, J.S. T'ien, P.V. Ferkul, S.L. Olson, M.C. Johnston, Flame growth around a spherical solid fuel in low speed forced flow in microgravity, Fire Technol. (2020), doi:10.1007/s10694-019-00848-2.
[16] J.G. Quintiere, Fundamental of Fire Phenomena, John Wiley, New York, 2006, doi:10.1002/0470091150.
[17] Q. Xie, R. Tu, N. Wang, X. Ma, X. Jiang, Experimental study on flowing burning behaviors of a pool fire with dripping of melted thermoplastics, J. Hazard. Mater. 267 (2014) 48–54, doi:10.1016/j.jhazmat.2013.12.033.
[18] X. Huang, Critical drip size and blue flame shedding of dripping ignition in fire, Sci. Rep. 8 (2018) 16528, doi:10.1038/s41598-018-34620-3.
[19] Y. Kobayashi, X. Huang, S. Nakaya, M. Tsue, C. Fernandez-Pello, Flame spread over horizontal and vertical wires: the role of dripping and core, Fire Saf. J. 91 (2017) 112–122, doi:10.1016/j.firesaf.2017.03.047.
[20] O. Fujita, K. Nishizawa, K. Ito, Effect of low external flow on flame spread over polyethylene-insulated wire in microgravity, Proc. Combust. Inst. 29 (2002) 2545–2552, doi:10.1016/S1540-7489(02)80310-8.
[21] J.-M.M. Citerne, H. Dutilleul, K. Kizawa, M. Nagachi, O. Fujita, M. Kikuchi, et al., Fire safety in space - investigating flame spread interaction over wires, Acta Astronaut. 126 (2016) 500–509, doi:10.1016/j.actaastro.2015.12.021.
[22] X. Huang, Y. Nakamura, D. Urban, Introduction to special issue on spacecraft fire safety, Fire Technol. 56 (2020) 1–4, doi:10.1007/s10694-019-00941-6.
[23] M. Ikeda, Effects of gravity on ignition and combustion characteristics of externally heated polyethylene film, Microgravity Sci. Technol. 30 (2018) 331–338, doi:10.1007/s12217-018-9606-9.
[24] H. Zhang, R. Fan, S. Wang, X. Tian, K. Xu, S. Wan, et al., Extinction of lean near-limit methane/air flames at elevated pressures under normal-and reduced-gravity, Proc. Combust. Inst. 33 (2011) 1171–1178, doi:10.1016/j.proci.2010.06.027.
[25] M. Tomaides, K.T. Whitby, Fine Particles : Aerosol Generation, Measurement, Sampling, and Analysis, 1st ed., Academic Press, New York, 1976.
[26] S.L. Olson, P.V. Ferkul, Microgravity flammability boundary for PMMA rods in axial stagnation flow: experimental results and energy balance analyses, Combust. Flame 180 (2017) 217–229, doi:10.1016/j.combustflame.2017.03.001.
[27] J. Walendziewski, M. Steininger, Thermal and catalytic conversion of waste polyolefines, Catal. Today 65 (2001) 323–330, doi:10.1016/S0920-5861(00)00568-X.
[28] J. Luche, E. Mathis, T. Rogaume, F. Richard, E. Guillaume, High-density polyethylene thermal degradation and gaseous compound evolution in a cone calorimeter, Fire Saf. J. 54 (2012) 24–35, doi:10.1016/j.firesaf.2012.08.002.
[29] S. Link, X. Huang, C. Fernandez-Pello, S. Olson, P. Ferkul, The effect of gravity on flame spread over PMMA cylinders, Sci. Rep. 8 (2018) 120, doi:10.1038/s41598-017-18398-4.
[30] K.T. Dotson, P.B. Sunderland, Z.G. Yuan, D.L. Urban, Laminar smoke points of coflowing flames in microgravity, Fire Saf. J. 46 (2011) 550–555, doi:10.1016/j.firesaf.2011.08.002.
[31] K.C. Lin, G.M. Faeth, Shapes of nonbuoyant round luminous laminar-jet diffusion flames in coflowing air, AIAA J. 37 (1999) 759–765, doi:10.2514/2.785.
[32] A. Markan, P.B. Sunderland, J.G. Quintiere, J.L. de Ris, D.P. Stocker, H.R. Baum, A burning rate emulator (BRE) for study of condensed fuel burning in microgravity, Combust. Flame 192 (2018) 272–282, doi:10.1016/j.combustflame.2018.01.044.
[33] Z. Dai, G.M. Faeth, Hydrodynamic suppression of soot formation in laminar coflowing jet diffusion flame, Proc. Combust. Inst. 28 (2000) 2085–2092.
[34] P. Sun, S. Lin, X. Huang, Ignition of thin fuel by thermoplastic drips: an experimental study for the dripping ignition theory, Fire Saf. J. 115 (2020) 103006, doi:10.1016/j.firesaf.2020.103006.
[35] M. Mizomoto, S. Ikai, A. Morita, Evaporation and ignition of a fuel droplet on a hot surface (Part 4, model of evaporation and ignition), Combust. Flame 104 (1983) 95–104, doi:10.1016/0010-2180(83)90086-X.
[36] M. Ghamari, A. Ratner, Combustion characteristics of diesel and Jet-A droplets blended with polymeric additive, Fuel 178 (2016) 63–70, doi:10.1016/j.fuel.2016.03.052.
[37] M.C. Hicks, V. Nayagam, F.a. Williams, Methanol droplet extinction in carbon–dioxide-enriched environments in microgravity, Combust. Flame 157 (2010) 1439–1445.
[38] S. Kumar, R.K. Singh, Thermolysis of high-density polyethylene to petroleum products, J. Petrol. Eng. 2013 (2013) 1–7, doi:10.1155/2013/987568.
[39] A. Tewarson, Flammability of polymers, Plastics and the Environment, John Wiley & Sons, Ltd, Hoboken, NJ, USA (2004), pp. 403–489, doi:10.1002/0471721557.ch11.
[40] C.K. Law, F.A. Williams, Kinetics and convection in the combustion of alkane droplets, Combust. Flame 19 (1972) 393–405, doi:10.1016/0010-2180(72)90009-0.
[41] Andrews J.R., Biblarz O. Temperature Dependence of Gas Properties in Polynomial Form. 1981.
[42] A.C. Cogley, S.C. Saxena, Thermal conductivity of methane at atmospheric pressure in the temperature range of 360-1275K, J. Heat Transf. 102 (1980) 163–167, doi:10.1115/1.3244230.
[43] T.L. Bergman, A.S. Lavine, F.P. Incropera, D.P. DeWitt, Fundamentals of Heat and Mass transfer, 2011, 13, John Wiley & Sons, USA (2015), pp. 470–978. ISBN.
[44] V. Nayagam, Quasi-steady flame standoff ratios during methanol droplet combustion in microgravity, Combust. Flame 157 (2010) 204–205, doi:10.1016/j.combustflame.2009.09.012.
[45] C.K. Law, S.H. Chung, N. Srinivasan, Gas-phase quasi-steadiness and fuel vapor accumulation effects in droplet burning, Combust. Flame 198 (1980) 173–198, doi:10.1016/0010-2180(80)90049-8.
[46] B.D. Shaw, F.L. Dryer, F.A. Williams, Sooting and disruption in spherically symmetrical combustion of decane droplets in air, Acta Astronaut. 17 (1988) 1195–1202, doi:10.1016/0094-5765(88)90008-2.
[47] S. Kumagai, T. Sakai, S. Okajima, Combustion of free fuel droplets in a freely falling chamber, Symp. (Int.) Combust. 13 (1971) 779–785, doi:10.1016/S0082-0784(71)80080-2.
[48] S. Ulzama, E. Specht, An analytical study of droplet combustion under microgravity: quasi-steady transient approach, Proc. Combust. Inst. 31 II (2007) 2301–2308, doi:10.1016/j.proci.2006.07.134.
[49] T. Farouk, F.L. Dryer, Tethered methanol droplet combustion in carbon-dioxide enriched environment under microgravity conditions, Combust. Flame 159 (2012) 200–209, doi:10.1016/j.combustflame.2011.06.014.
[50] A.J. Marchese, F.L. Dryer, R.O. Colantonio, V. Nayagam, Microgravity combustion of methanol and methanol/water droplets: drop tower experiments and model predictions, Symp. (Int.) Combust. 26 (1996) 1209–1217, doi:10.1016/S0082-0784(96)80337-7.